Carrier relaxation dynamics of $Zn_xCd_{1-x}Se/C$ core/shell nanocrystals with phase separation as studied by time-resolved cathodoluminescence

Y. Estrin,[1] D. H. Rich,[1,a)] O. Moshe,[1] Sayan Bhattacharyya,[2] and A. Gedanken[2]
[1]*Department of Physics, The Ilse Katz Institute for Nanoscience and Nanotechnology, Ben-Gurion University of the Negev, P.O. Box 653, Beer-Sheva 84105, Israel*
[2]*Department of Chemistry, Kanbar Laboratory for Nanomaterials at the Bar-Ilan University Center for Advanced Materials and Nanotechnology, Bar-Ilan University, Ramat-Gan 52900, Israel*

(Received 3 September 2009; accepted 11 October 2009; published online 2 November 2009)

The optical properties and carrier relaxation kinetics of $Zn_xCd_{1-x}Se/C$ core/shell nanocrystals with compositional phase separation occurring on a ~1–5 nm size scale were examined with time-resolved cathodoluminescence (CL) spectroscopy and imaging. The CL spectral lineshape was found to depend on the level of excitation, temperature, and the time-window during time-delayed spectroscopy. The kinetics of carrier thermalization and transfer between Cd-rich phase-separated regions and the homogenous ZnCdSe alloy were examined. We show that the rare phenomenon of compositional phase separation in II-VI nanocrystals leads to interesting and potentially useful optical properties. © *2009 American Institute of Physics*. [doi:10.1063/1.3257975]

Much effort has been expended recently in studying the synthesis of variable gap $Zn_xCd_{1-x}Se$ materials in the form of nanowires,[1,2] nanorods,[3] and nanocrystals.[4] The chemical phase separation during the growth and synthesis of strained ternary semiconductors can yield additional quantum effects if the spatial modulation is less than ~10 nm, and possibly provide for additional device applications such as, e.g., the spontaneous formation of quantum wires during the growth of $(InP)_2/(GaP)_2$ bilayer superlattices on GaAs.[5–7] Chemical phase separation within ternary II-VI crystals is a rare phenomenon, but has been predicted and observed.[8] Using high-resolution transmission electron microscopy (TEM), a spinodal-like phase separation was observed for $Cd_xZn_{1-x}Te$ layers grown on GaAs substrates.[9]

In our recent study of $Zn_xCd_{1-x}Se/C$ core-shell nanocrystals, TEM showed two-dimensional (2D) striations in the nanocrystals that are indicative of a composition modulation along a preferred crystallographic direction and reveal a chemical phase separation.[10] CL of these nanocrystals further showed that a composition modulation, Δx, of ~0.11 is consistent with a broadened emission and set of decomposed peaks in spatially integrated CL spectra.[10] In this letter, we further build on the results of phase separation in $Zn_xCd_{1-x}Se$ nanocrystals by examining the carrier relaxation dynamics with time-resolved CL. Unexpected phenomena, such as phase separation in II-VI nanocrystals, may provide a means to create lower dimensional quantum structures.

$Zn_xCd_{1-x}Se/C$ core/shell nanocrystals with 31–39 nm cores and 11–25 nm thick carbon shells were synthesized from solid state precursors in large scale amounts. A mixture of spherical and tripod nanostructures were obtained in a one-step reaction with our sample label ZC3.[10] A subsequent x-ray diffraction (XRD) Rietveld analysis that identified the relative Zn composition, x, and cubic and hexagonal structural phases has been previously reported.[10] The CL experiments were performed on a modified JSM-5910 scanning electron microscope (SEM) with an e-beam energy (E_b) of 15 keV. The time-resolved CL detection system and method have been described previously in detail.[11]

Figure 1(a) shows bright-field TEM images of single nanocrystals from two different regions of the sample. A hexagonal ~31 nm core is shielded by a ~8 nm carbon shell in the left image. Significant striations are observed in both nanocrystals, as seen in the figure. These striations indicate a composition modulation and spinodal decomposition within the nanocrystals, with such fluctuations occurring on a ~1–5 nm size scale. Therefore, such a phase separation occurs within the quantum confinement regime for electrons and holes in the nanocrystal and leads to expected local modifications of the optical and electronic properties. In Fig. 1(b), we show spatially averaged CL spectra for T=60 K over the region represented by the SEM image of Fig. 1(c).

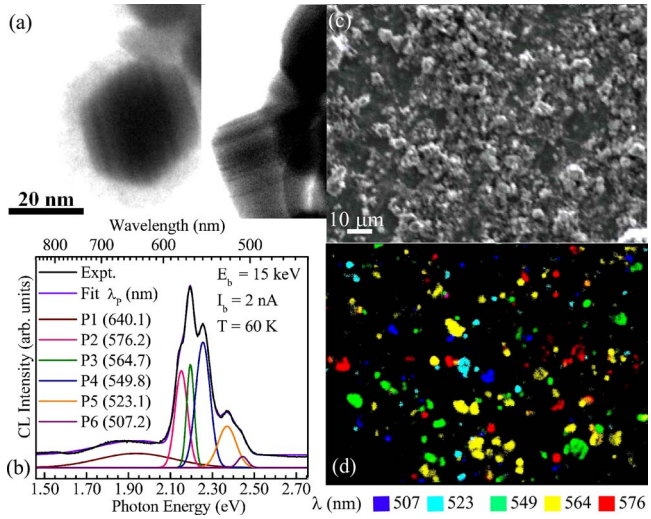

FIG. 1. (Color online) Bright-field TEM images of two different $Zn_xCd_{1-x}Se/C$ nanocrystals in (a). Spatially integrated CL spectrum (with a ~1 nm spectral resolution) and the decomposition into Gaussian components P_1-P_6 in (b), as previously described in Ref. 10. SEM image of the region over which the spatially integrated CL spectra and monochromatic CL images were acquired in (c). A composite CL image that maps the emission of groups of nanocrystals that possess similar peak emission wavelengths in (d).

a)Electronic mail: danrich@bgu.ac.il.

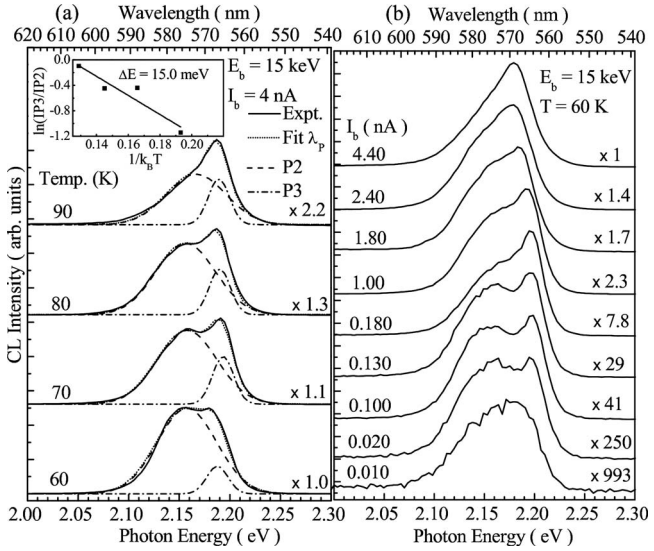

FIG. 2. A stack plot of CL spectra acquired by local excitation of $Zn_{0.47}Cd_{0.53}Se$ nanocrystals at various temperatures in (a). A semilog plot of $\ln(I_{P3}/I_{P2})$ vs $1/k_BT$ is shown as an inset. CL spectra acquired for local excitation of a similar group of nanocrystal for various beam currents I_b in (b).

The CL spectrum was decomposed into a sum of discrete Gaussian peaks, as indicated by the labels P_1–P_6 in Fig. 1(b).[10] Previously, using XRD and the compositional dependence of the $Zn_xCd_{1-x}Se$ band gap emission energy, we attributed peak P_3 (564.7 nm) as due to a combination of emissions from nanocrystals possessing homogenous compositions, x, of ~0.47 (h) and ~0.50 (c), in which h and c refer to the hexagonal and cubic phases, respectively.[10] Moreover, peaks P_2 (576.2 nm) and P_4 (549.8 nm) correlate with emissions from regions exhibiting phase separation into compositions of 0.41 (h) and 0.52 (h), respectively.[10]

In order to study the carrier dynamics in the nanocrystals, we have further mapped the monochromatic images with wavelengths corresponding to the decomposed peaks, P_2–P_6, into a composite false-color image, as shown in Fig. 1(d). We observed that groups of nanocrystals within regions of constant wavelength (i.e., false color) exhibit very similar local CL spectra, in which the e-beam remains fixed during the acquisition of a CL spectrum. In Fig. 2, we show such CL spectra acquired with localized excitation when the e-beam was focused on a region represented by an intense P_3 (564.7 nm) emission. Figure 2(a) shows the temperature dependence of such local CL spectra for a fixed beam current (I_b) of 4 nA. The spectral lineshape exhibits an increasing asymmetry as the temperature is raised from 60 to 90 K. In order to better quantify the change in asymmetry we decomposed the lineshapes into the two Gaussian components, P_2 and P_3, in a manner similar to that shown in Fig. 1(b). The intensity of the longer wavelength P_2 component decreases relative to that of P_3 as the temperature increases from 60 to 90 K, suggesting that carrier excitation from the phase-separated region to the homogenous regions [$x \approx 0.47$ (h)] of the nanocrystal occurs over this temperature range.

In order to test this hypothesis, we can expect an Arrhenius dependence of the form $I_{P3}/I_{P2} \propto \exp-(\Delta E_a/k_BT)$, where I_{P2} and I_{P3} are the integrated intensities of the Gaussian components and ΔE_a is an activation energy associated with the energy barrier separating electrons and holes in the lower band gap Cd-rich region from the homogenous $Zn_{0.47}Cd_{0.53}Se$ region, without phase separation. The inset of Fig. 2(a) exhibits a plot of $\ln(I_{P3}/I_{P2})$ versus $1/k_BT$, from which $\Delta E_a = 15.0 \pm 3.7$ meV is extracted from a linear fit. The excitation of correlated electron–hole pairs from the Cd-rich region to the homogenous alloy ($x \approx 0.47$ and without phase separation) is possible in the strong confinement regime, when Coulomb-induced electron–hole correlations are weak.[12] If carriers are re-emitted as correlated electron–hole pairs from confined regions, then according to the requirements of detailed balance during a steady-state excitation, the measured activation energy would be about half of the total barrier height.[13] The latter appears to represent the present case since the average energy difference between peaks P_2 and P_3 in Fig. 2(a) is 32.3 meV, which represents the total barrier height, and is therefore approximately twice the measured ΔE_a.

Figure 2(b) shows the excitation dependence for various I_b at T=60 K in a similar but not identical group of nanocrystals that yielded the results of Fig. 2(a). For the lowest beam current shown, $I_b = 10$ pA, a single broad luminescence peak rapidly evolves into the expected double-peaked lineshape observed in Fig. 2(a). The onset of the increase in intensity of the higher-energy component (i.e., the P_3 component) for $I_b \geq 180$ pA reflects the rapid phase and real space filling of states in the Cd-rich regions, leading to an enhanced carrier transfer to the homogenous alloy. The average 2D carrier density, n, in a $Zn_{0.47}Cd_{0.53}Se$ nanocrystal with a 35 nm-thick core and ten Cd-rich 2D regions (as evidenced from the ~10 striations per nanocrystal in the TEM images of Fig. 1) is estimated as $n \approx I_b \cdot 2.5 \times 10^{12}$ cm^{-2} with the e-beam current in units of nA.[14,15] A carrier density of $\sim 4.5 \times 10^{11}$ cm^{-2} at $I_b = 180$ pA yields a *nonequilibrium* electron Fermi energy, E_F, of 8.1 meV above the band edge at T=60 K, assuming that the Cd-rich regions behave as quantum wells surrounded by Zn-rich barriers.[16] Thus, the relative increase of the intensity of P_3 for $I_b > \sim 180$ pA correlates with an excitation level in which $E_F(T)$ begins to approach the value of the activation energy, ΔE_a, during which thermal excitation of carriers from the Cd-rich region to the homogenous alloy becomes energetically more favorable. For excitations $I_b > \sim 1$ nA, a further smearing of the P_2 and P_3 components is observed and reflects an enhanced carrier transfer between the phase-separated and homogenous regions.

A stack plot of intensity versus time transients is shown in the semilog plot of Fig. 3(a) for various wavelengths. From the transients, we have extracted the decay time in the usual manner with a linear fit in the decay regions for various wavelengths. We show a detailed plot of the decay time versus wavelength for sample temperatures of 60, 90, and 100 K in Fig. 3(b). The decay times appear to be relatively independent of temperature, within the error bar, for the three temperatures shown. The decay times appear roughly constant at ~0.6 ns within the scatter for 560 nm $\leq \lambda \leq \sim 575$ nm, but rapidly increase for $\lambda \geq \sim 580$ nm.

The increase in lifetime for the longer wavelength Cd-rich regions reflects a reduction in e-h oscillator strength. An additional contribution to the increase in lifetime for this region may also stem from thermalization of carriers from the higher-energy states of the homogenous alloy (P_3 component) to the lower energy states in the Cd-rich region

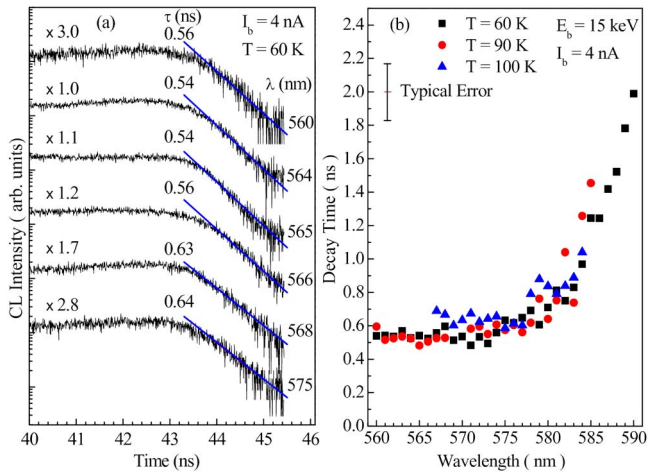

FIG. 3. (Color online) CL intensity vs time transients for various wavelengths for local excitation of a group of $Zn_{0.47}Cd_{0.53}Se$ nanocrystals in (a). CL decay time vs wavelength for various temperatures in (b).

(P_2 component). In order to test this hypothesis, we have measured time-delayed CL spectra for the e-beam injection into the nanocrystals. The time-delayed spectra were constructed from the full set of CL transients in the 545 nm $\leq\lambda\leq$600 nm range at temperatures of 60 and 90 K, as shown in Figs. 4(a) and 4(b), respectively. The spectra labeled *in pulse* were constructed using a time window near the center of the excitation pulse in which a steady-state condition was reached. Thus, the *in pulse* spectra ought to closely resemble the constant excitation CL spectra of Fig. 2, which is the case. For the set of time-delayed spectra at both temperatures, we observe that the intensity of the P_3 component decreases relative to that of P_2 as *snapshot*s are acquired

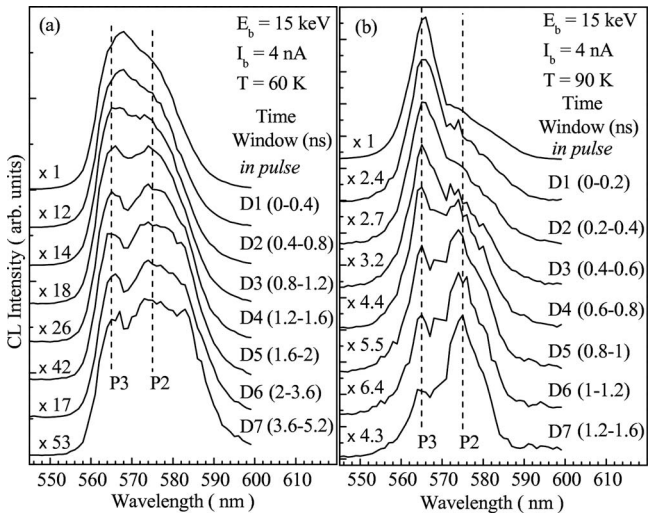

FIG. 4. Time delayed CL spectra for the local excitation of a group of $Zn_{0.47}Cd_{0.53}Se$ nanocrystals at temperatures of 60 K (a) and 90 K (b). Various time windows D1-D7 reveal snapshots of the CL spectrum during the decay.

at longer time windows (D*i*) after the decay edge, as labeled D1–D7 in Fig. 4. However, the rate of decrease of P_3 relative to P_2 is more pronounced for the case of T=90 K, as the P_2 component is observed to dominate P_3 in the D5 to D7 time windows of Fig. 4(b). This behavior is consistent with carriers diffusing and thermalizing from the higher-energy homogenous alloy region (P_3) of the nanocrystals to the lower-energy phase-separated region (P_2) after the trailing edge of the e-beam excitation pulse. The rapid change in the relative contributions of the P_2 and P_3 components with temperature strongly suggests that carrier thermalization between the two regions plays an essential role in the decay kinetics.

In conclusion, the optical properties and carrier relaxation kinetics of $Zn_xCd_{1-x}Se/C$ core/shell nanocrystals with a compositional phase separation were examined with time-resolved CL. The CL spectral lineshape was found to depend on the excitation level, temperature, and time-window during time-delayed spectroscopy. Variations in the lineshape with temperature were found to be consistent with the carrier transport and thermalization between the phase-separated and homogenous $Zn_{0.47}Cd_{0.53}Se$ alloy regions in the nanocrystals. These results illustrate that compositional phase separation in II-VI nanocrystals can lead to potentially useful quantum effects and optical properties.

[1]X. T. Zhang, Z. Liu, Q. Li, and S. K. Hark, J. Phys. Chem. B **109**, 17913 (2005).
[2]R. Venugopal, P. I. Lin, and Y.-T. Chen, J. Phys. Chem. B **110**, 11691 (2006).
[3]H. Lee, P. H. Holloway, H. Yang, L. Hardison, and D. Kleiman, J. Chem. Phys. **125**, 164711 (2006).
[4]Y.-M. Sung, Y.-J. Lee, and K.-S. Park, J. Am. Chem. Soc. **128**, 9002 (2006).
[5]K. C. Hsieh, J. N. Baillargeon, and K. Y. Cheng, Appl. Phys. Lett. **57**, 2244 (1990).
[6]A. Mascarenhas, R. G. Alonso, G. S. Horner, S. Froyen, K. C. Hsieh, and K. Y. Cheng, Phys. Rev. B **48**, 4907 (1993).
[7]Y. Tang, D. H. Rich, A. M. Moy, and K. Y. Cheng, J. Vac. Sci. Technol. B **15**, 1034 (1997).
[8]A. Marbeuf, R. Druilhe, R. Triboulet, and G. Patriarche, J. Cryst. Growth **117**, 10 (1992).
[9]H. S. Lee, H. S. Sohn, J. Y. Lee, K. H. Lee, Y. H. Kim, T. W. Kim, M. S. Kown, and H. L. Park, J. Appl. Phys. **99**, 093512 (2006).
[10]S. Bhattacharyya, Y. Estrin, O. Moshe, D. H. Rich, L. A. Solovyov, and A. Gedanken, ACS Nano **3**, 1864 (2009).
[11]H. T. Lin, D. H. Rich, A. Konkar, P. Chen, and A. Madhukar, J. Appl. Phys. **81**, 3186 (1997).
[12]G. W. Bryant, Phys. Rev. B **37**, 8763 (1988).
[13]W. Yang, R. R. Lowe-Webb, H. Lee, and P. C. Sercel, Phys. Rev. B **56**, 13314 (1997).
[14]K. Kanaya and S. Okayama, J. Phys. D: Appl. Phys. **5**, 43 (1972).
[15]We have estimated the generation rate, G, of carriers in a spherical $Zn_{0.47}Cd_{0.53}Se$ nanocrystal with a volume of 2.2×10^4 nm^3 under a 15 keV e-beam excitation condition using the standard model which uses a material-dependent normalized one-dimensional depth dose curve, as described in Ref. 14. From this estimation $G\approx4.3\times10^{11}$ s^{-1} for a 1 nA e-beam current and $\tau\approx0.6$ ns from the time-resolved CL measurements.
[16]The Fermi energy for a 2D system is given by $E_F=k_BT\ln[\exp(\pi\hbar^2n/m_ek_BT)-1]$, where $m_e\approx0.12$ m_0 for $Zn_{0.47}Cd_{0.53}Se$, from O. Madelung, *Semiconductors—Basic Data*, 2nd ed. (Springer, New York, 1996).